Korean J. Chem. Eng., 39(12), 3315-3322 (2022)
DOI: 10.1007/s11814-022-1262-5

pISSN: 0256-1115
eISSN: 1975-7220

Performance evaluation of zero-gap vanadium redox flow battery using composite electrode consisting of graphite and buckypaper

Kyuhwan Hyun*, Mingyu Shin, and Yongchai Kwon*,**,***,†**

*Energy & Environment Research Institute, Seoul National University of Science and Technology, 232 Gongneung-ro, Nowon-gu, Seoul 01811, Korea
**Department of Chemical and Biomolecular Engineering, Seoul National University of Science and Technology, 232 Gongneung-ro, Nowon-gu, Seoul 01811, Korea
***Department of Energy and Chemical Engineering, Seoul National University of Science and Technology, 232, Gongneung-ro, Nowon-gu, Seoul 01811, Korea
(*Received 17 June 2022 • Revised 12 August 2022 • Accepted 17 August 2022*)

Abstract−A composite electrode consisting of graphite felt and buckypaper (GF-BP) was developed. GF-BP is used for fabricating a zero-gap structure for all-vanadium redox flow battery (VRFB), which minimizes the distance between two electrodes. With this zero-gap structure, performance of VRFBs is improved, while its flexible design becomes possible. GF and BP are used as base and reinforced materials to combine the proper porous structure of GF and the excellent redox reactivity of vanadium ions promoted by BP. The properties of GF-BP electrode and its applicability to VRFB were evaluated electrochemically and spectroscopically. As a result, its total pore volume and double layer capacitance (0.200 cm^3 g^{-1}, 1,547.95 mF g^{-1}) are higher than those of pristine GF electrode (0.040 cm^3 g^{-1}, 94.59 mF g^{-1}). When the optimized GF-BP electrode and zero-gap structure are adopted, performance of the zero-gap VRFB using the optimized GF-BP electrode is excellent with energy efficiency (EE) of 60% and discharge capacity of 14.6 Ah L^{-1} at 160 mA cm^{-2}, while the EE (67.8%) is 20% better than that using pristine GF electrode (72.4%) at 120 mA cm^{-2}. The significant increase in actual active sites of the optimized GF-BP electrode is the main reason for the performance enhancement of the zero-gap VRFB using this.

Keywords: Zero-gap Structure, Buckypaper, Vanadium Redox Flow Battery, Carbon Nanotube, Graphite Felt

INTRODUCTION

Renewable energies are essential energy sources to overcome the fatal problems occurring by excessive coal consumption, while they can offer benefits regarding cleanness and sustainability [1,2]. However, when renewable energies are used, electric grids are limited because the power produced from the renewable energy is intermittent and irregular [3]. To alleviate the drawback of renewable energy, establishing large-scale energy storage systems (ESSs) is required [4]. ESS stores various types of energies and then uses them when needed. As the ESS devices, lithium-battery, redox flow battery, flywheel, and supercapacitor have been mainly considered so far [5-10]. These have played a critical role in minimizing the overloading and frequency fluctuation of renewable energy [11,12]. Each ESS device has its pros and cons related to power density, energy density, and safety. Of the candidates, recently, redox flow batteries (RFBs) have received deep attention thanks to their high energy storage capacity, and low explosion and fire risks despite their low energy density [7,13-15].

Among the various RFBs, the most studied are the all-vanadium redox flow batteries (VRFBs) [16-18]. VRFB uses vanadium ions as active material for both anolyte and catholyte. This can produce a cell voltage of ~1.26 V, and its solubility in sulfuric acid (H_2SO_4) is 1.8 M, which is higher than that of other active materials used for RFB [19,20]. In addition, since the vanadium ions are used for both electrolytes, the capacity loss of VRFB occurring by crossover of vanadium ions is considerably reduced [21-23]. However, in spite of these advantages, the conventional cell design of VRFB still has some limitations [24-26]. One of the limitations is its thick electrode. For example, when graphite felt (GF) electrode is used, its thickness is too thick as 3-5 mm [27-29]. When such a thick electrode is used in VRFB, areal specific resistance (ASR) of the cell is higher than when thin electrode is used, while the pathway of charges of active materials is long, and such long a transport path and ASR may weaken the redox reactivity of active materials and the power density of VRFB [24,30].

For the above reason, recently, there have been some efforts to develop thin electrode (e.g., carbon papers) for VRFB [24,26,30,31]. When the thin electrode is used, both ASR of VRFB and the distance for transport path of charges of active material are reduced, and these can promote the redox reactivity of active material and the power density of VRFB. VRFBs using thin electrode are denoted as zero-gap VRFBs [32,33].

Since these zero-gap VRFBs have the above benefits, there have been researches. Zeng et al. used thin and porous polybenzimidazole (PBI) membrane with a porous layer for VRFB [34]. With that,

†To whom correspondence should be addressed.
E-mail: kwony@seoultech.ac.kr

the permeability and thickness of membranes could be optimized. Xu et al. suggested zero-gap electrode including micron- and nano-scale structure for VRFB to increase the catalytic effect and electron transfer [35]. Wei et al. used electrocatalysts consisting of hollow Ti_3C_2Tx spheres on divided GFs for VRFB to enhance electrical conductivity of active materials [36]. With that, the redox reactivity of V^{3+}/V^{2+} reaction was enhanced in the zero-gap structure.

Although the performance of VRFBs was improved by the above researches, they had still serious drawbacks. For example, for incorporating the above researches, complicated catalyst manufacturing and electrode preparation processes were required. In addition, their fabrication cost was expensive.

In this study, to overcome the above problems of VRFBs and further improve their performance, a new composite electrode consisting of graphite felt and buckypaper (GF-BP) is suggested. Buckypaper (BP) has clear pros and cons [37-40]. This is a sheet of thin thickness attributed to carbon nanotube and has excellent flexibility. However, since its density is higher than that of other carbon-based electrodes, permeability of charge carriers within electrolytes through BP is very low. To alleviate the permeability issue of charge carriers, GF is considered as a reinforced material [41-43]. With the use of GF and BP, the thickness of electrode is preserved, while its flexibility is improved.

Based on the above advantages, properly manufactured GF-BP

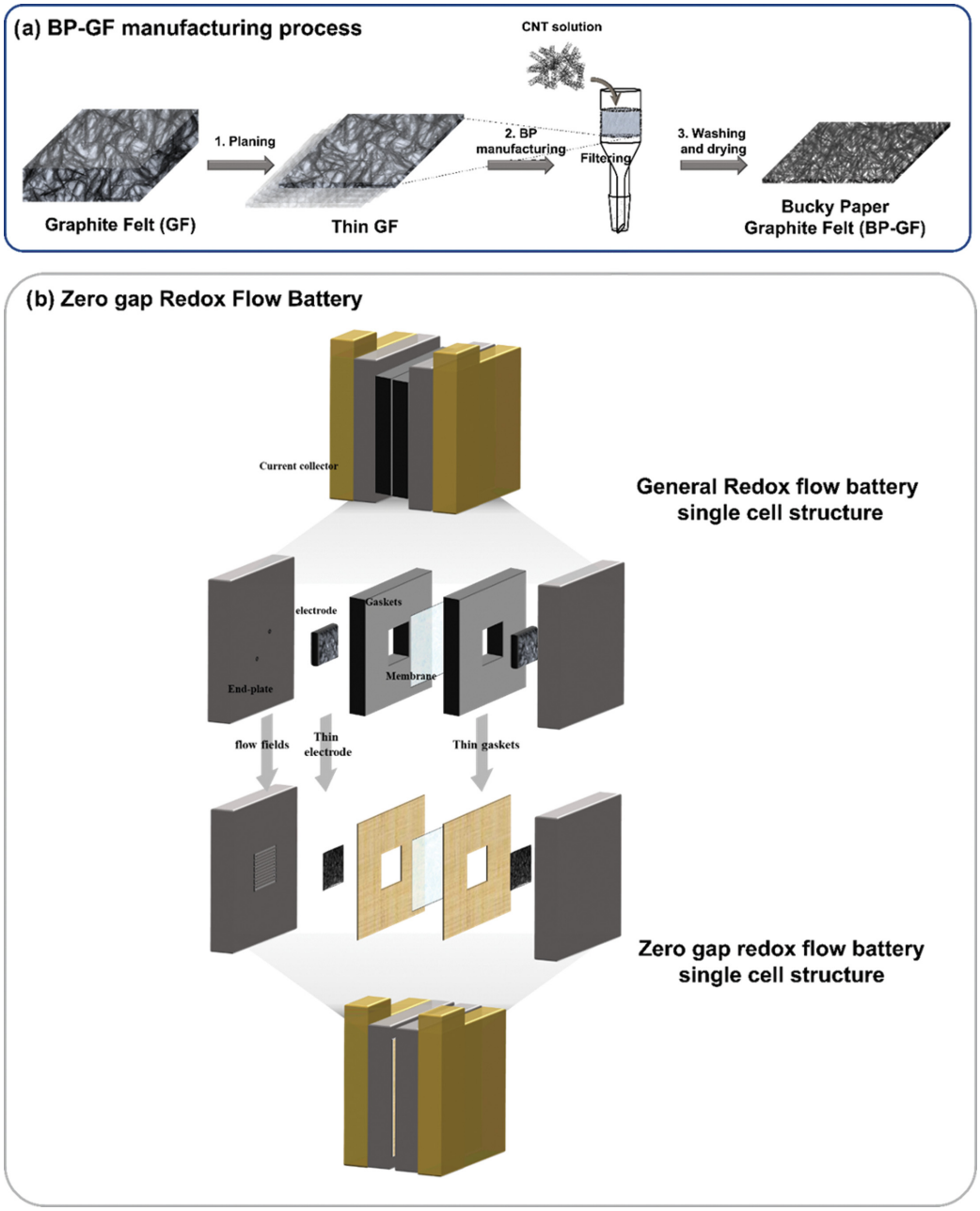

Scheme 1. (a) Schematics showing the manufacturing process of BP-GF electrode, and (b) difference in cell structure of general RFB and zero gap RFB single cells.

electrodes were prepared. Their properties were electrochemically and chemically evaluated, while double layer capacitance and cyclic voltammetry were used for the electrochemical evaluation, and SEM and BET were used for the structural analysis. The charge-discharge curves were used to measure the performance of VRFBs using the corresponding electrodes.

EXPERIMENTAL

1. Materials

Vanadium (IV) oxide sulfate hydrate (97%), Sodium dodecylbenzenesulfonate (SDBS, technical grade), and Nafion 117 solution (~5% in a mixture of lower aliphatic alcohols and water) were purchased from Sigma-Aldrich and used without further purifications. Sulfuric acid (95.0%) and 2-propanol (isopropyl alcohol, IPA, 99.5%) were purchased from Samchun Chemical (Korea) and used without further purifications. Multi-walled carbon nanotube (MWCNT, outer diameter: 5-15 nm) were from Avention (Korea) and used. As membrane that was used for this study, Nafion 117 (purchased from Chemours™ (USA)) was used, while SIGRACELL® Battery Felts (GFD 4.6) manufactured by SGL Carbon SE (Germany) was considered as GF electrode.

2. Preparation and Structural Characterization of New Electrodes

Three electrodes were prepared for this study, denoted as BP-GF, CNT/GF and BP. For producing BP-GF electrode, 160 mg SDBS was initially dispersed into 100 mL DIW, and the solution was sonicated for 5 min. Then, 80 mg of MWCNT was included into the above solution, and a new solution including MWCNT particles was sonicated for 5 min to increase the distribution capability of the MWCNT particles. Such sonicated solution was then vacuum filtrated using cellulose acetate filter (Advantec membrane filter, 0.45 μm pore size, 47 mm diameter). Then, polyacrylonitrile (PAN) based GF substrate (GFD 4.6, Sigracell) was sliced to 1mm thickness, and this thin GF substrate was put on the cellulose acetate filter to form BP layer onto the GF substrate (Scheme 1(a)) [40].

For forming CNT/GF electrode, 40 mg MWCNT was dispersed into 5 mL IPA, and 20 mL Nafion 117 solution was further included. Such produced solution was sonicated for 5 min to increase the distribution capability of the MWCNT particles. Then, GF substrate is included into the solution containing MWCNT particles and stirred for 24 h. Over time, MWCNT particles are supposed to be stuck to the surface of GF. When the coating process of MWCNT particles onto GF substrate was well completed, the solution became transparent. Such formed CNT/GF was then collected and dried in the vacuum oven for 24 h at 70 °C. The manufacturing procedure of BP electrode is very similar to that of BP-GF electrode. Only difference is that BP electrode does not import GF substrate.

To examine the surface properties of such formed electrodes, Brunauer-Emmett-Teller (BET) was used [44,45]. The data collected by BET measurements was examined by using a special surface analyzer (BELSORP-mini II, BEL Japan). Furthermore, SEM (JSM-7610F, JEOL) was considered surficial feature of electrodes.

3. Electrochemical Characterizations of New Electrodes

Electrochemical properties of the electrodes were evaluated using cyclic voltammetry (CV) measurements. Bio-Logic VSP-128 potentiostat was used to obtain their CV graphs. A three-electrode cell was configured for the CV tests. Each of electrode was used as working electrode (0.5 cm^2), while silver chloride electrode (Ag/AgCl) and Pt wire were used as reference and counter electrodes [46]. For preparing for proper electrolytes, 1.5 M $VOSO_4$+3 M H_2SO_4 and 1.5 M V^{3+}+3 M H_2SO_4 were fabricated. Then, 1 mL in each of the electrolyte was extracted and they were diluted by 19 mL of 3 M H_2SO_4. Of the two electrolytes, 1.5 M V^{3+}+3 M H_2SO_4 was obtained by electrochemical oxidization of 1.5 M $VOSO_4$+3 M H_2SO_4 [47,48]. For the CV measurements of catholyte, the scanned potential range was 0.2-1.4 V vs. Ag/AgCl, while that was −0.9-0 V vs. Ag/AgCl for anolyte. The potential scan rate used was 50 mV s^{-1} [4,49].

For DLC analysis of electrodes, their CV curves were measured. Here, 3 M H_2SO_4 was considered as electrolyte, while the different potential scan rates of 5, 10, 20 and 30 mV s^{-1} were used and the scanned potential range was 0.0-0.4 V vs. Ag/AgCl.

4. Performance Evaluation of VRFB Single Cells Using the Corresponding Electrodes

VRFB single cell tests were conducted to measure and compare the effects of three electrodes (pristine GF, CNT/GF, and GF-BP electrodes) on the performance of VRFBs (Scheme 1(b)). Each electrode was used as both cathode and anode (active area of 4 cm^2). The electrolyte tank was filled with 17 mL of electrolyte, and Nafion 117 (Chemours, USA) was used as ion exchange membrane. The first step of VRFB single cell tests was to charge active materials up to 1.7 V (pre-activation step). After that, catholyte was removed and refilled by 17 mL of 1.5 M $VOSO_4$+3 M H_2SO_4 solution. Then, charging and discharging steps were run. The cut-off voltage was set from 1.65 V (for charging) to 0.8 V (for discharging), and the operating current densities were in the range of 40 to 200 mA cm^{-2}. All the experiments were carried out under N_2 purge state.

RESULTS AND DISCUSSION

1. Structural Evaluation of New Electrodes

To increase the synergetic effect of the appropriate porosity of GF and the excellent reactivity of BP, thin GF was used as a base material and BP was coated onto the thin GF (GF-BP electrode).

As control groups of GF-BP electrode, pristine BP, 1mm thick pristine GF, and CNT doped GF (CNT/GF) electrodes were considered. To optically inspect the state of each electrode, their SEM images were taken (Fig. 1). As shown in Figs. 1(a) and 1(b), in CNT/GF electrode, CNTs were partially covered onto the carbon fiber of GF substrate. Furthermore, some CNTs were agglomerated. This means that when the same amount of CNT is doped to GF substrate, CNTs in CNT/GF electrode are agglomerated and, thus, they cannot act as the active sites for redox reaction of vanadium ions. Figs. 1(c) and 1d show SEM images of pristine BP electrode. Its surface is very uniform and CNTs within pristine BP are tightly packed. Despite such benefits, the surface density of pristine BP electrode was so high that this was not porous enough. Such a tightly packed pristine BP may prevent a facile flowing of electrolyte, followed by the mass transfer of electrolyte, while its overpotential may increase.

In contrast to BP electrode, the surface density of GF-BP elec-

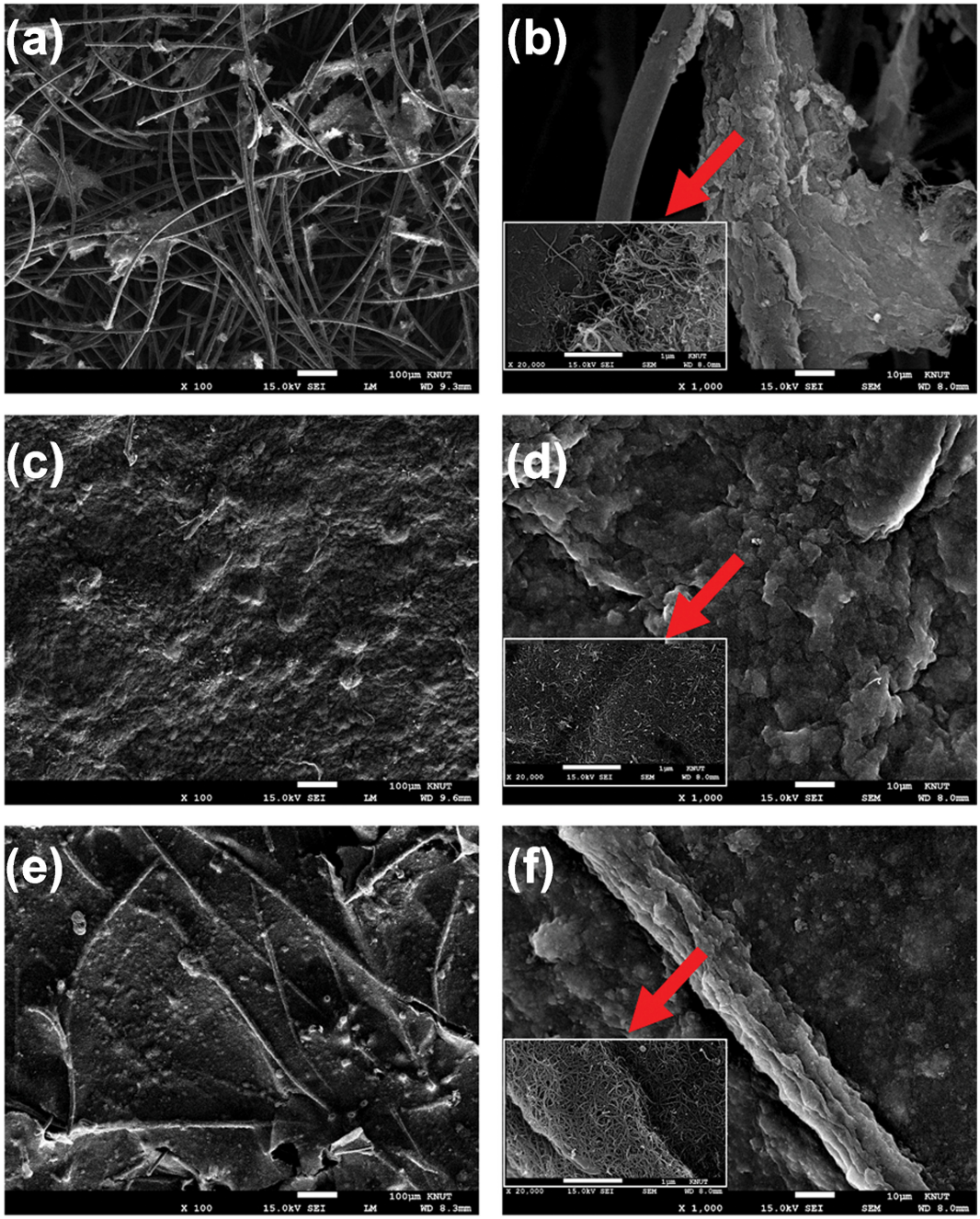

Fig. 1. SEM images of (a) and (b) CNT doped graphite felt, (c) and (d) buckypaper, (e) and (f) graphite felt-buckypaper composite electrodes.

trode is not excessively high (Figs. 1(e) and 1(f)). This is because carbon fibers of GF substrate are porous enough and, thus, when thin BP layer is well covered onto the carbon fibers of GF substrate, the surface density of such prepared GF-BP electrode is not excessively high.

With that, it is summarized that the porosity of GF-BP electrode is better than that of pristine BP electrode, while the uniformity of CNT doped onto GF-BP electrode is better than that of CNT/GF electrode. Thus, it is expected that the active surface area of GF-BP electrode will be larger than that of CNT/GF electrode.

To confirm the above expectations regarding the porosity and active surface area of electrodes, nitrogen adsorption and desorption of each sample was measured, and the electrode surface area was calculated using the BET isotherm (Fig. 2 and Table 1).

According to the analysis, the active surface area of BP-GF and CNT/GF electrodes was larger than that of pristine GF electrode. Furthermore, although the equivalent amount of CNT was loaded, the specific surface area of CNT/GF electrode (7.3984 m^2g^{-1}) was 35% larger than that of BP-GF electrode (10.055 m^2g^{-1}). Regarding pore size distribution, BP-GF electrode showed well-distributed pore size due to the uniformly dispersed CNTs (Fig. 2(b)). In addition, in average pore diameter, that of CNT/GF electrode (35.6 nm) was

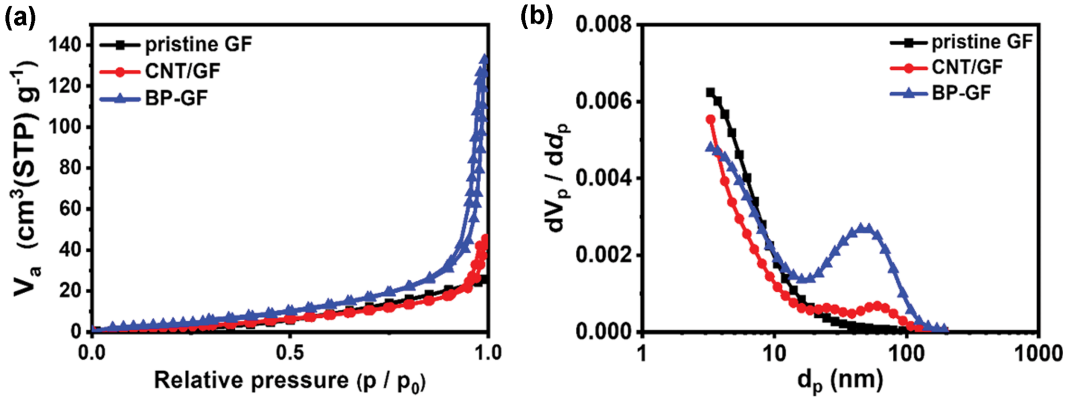

Fig. 2. (a) BET adsorption and desorption graphs of electrode samples. (b) Pore size distribution graphs of pristine GF, CNT/GF, BP-GF electrodes.

Table 1. Data measured by BET of each electrode sample

	Pristine GF	CNT/GF	BP-GF
Specific surface area (m^2 g^{-1})	1.5382	7.3984	10.055
Total pore volume (cm^3 g^{-1})	0.03958	0.06585	0.1997

smaller than that of BP-GF electrode (79.4 nm). This trend was well matched with that observed by SEM. Namely, in BP-GF electrode, as CNTs were dispersed uniformly, its active and specific surface areas increased.

Besides structural properties of the electrodes, their electrochemical performance was evaluated to estimate whether the electrodes were appropriate for VRFBs. Furthermore, it was necessary to investigate that the trend in specific surface area measured in Fig. 2 is well matched with that in electrochemical reactivity of vanadium ions contacting the electrodes.

To measure the electrochemical reactivity of vanadium ions, double layer capacitance (DLC) was calculated by measuring CV curve (Fig. 3 and Table 2) [50]. DLC is an indicator determining electrochemical active surface area (ECSA). To calculate this DLC, the current of each electrode sample was measured at various scan rates. Here, the current was collected in the region where a non-

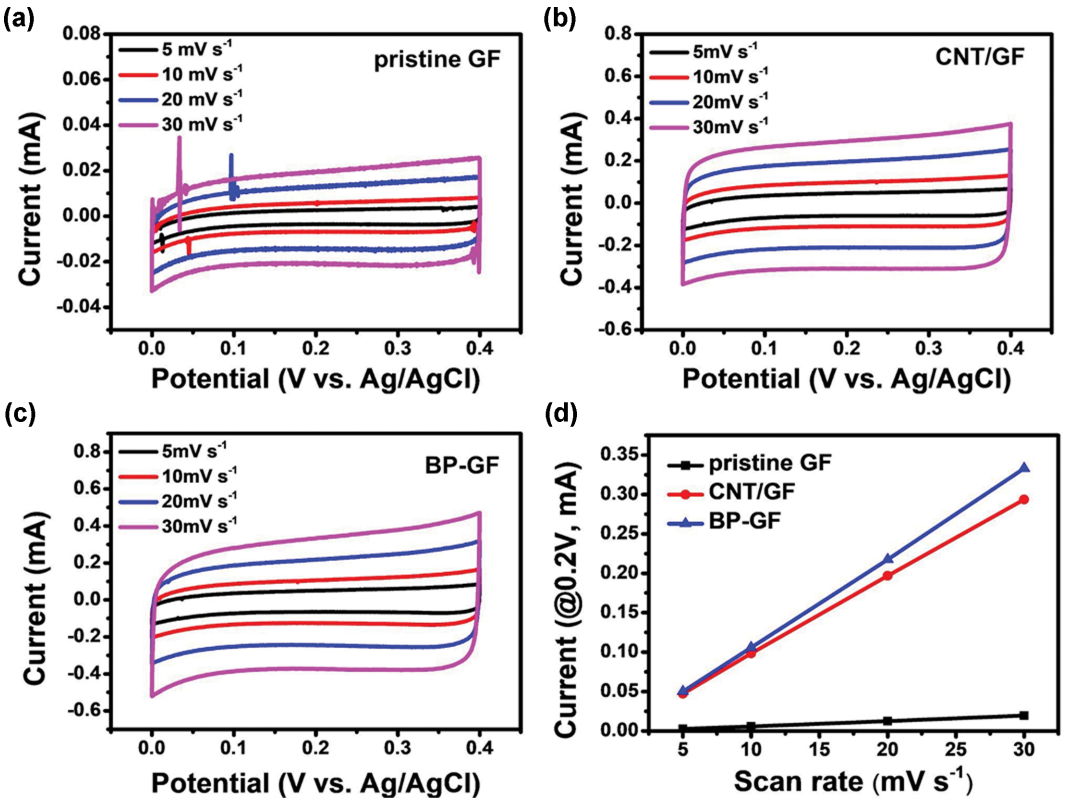

Fig. 3. Non-faradaic CV curves of (a) pristine GF, (b) CNT/GF, (c) BP-GF electrodes, and (d) double layer capacitance data of each electrode.

Table 2. Double layer capacitance data of each electrode sample

	pristine GF	CNT/GF	BP-GF
Double layer capacitance ($mF\ g^{-1}$)	94.59	1,256.41	1,547.95

faradaic reaction occurred.

$$\text{DLC (F)} = \frac{\text{Current (mA)}}{\text{Scan rate (mV/s)}}$$

As a result, DLC in pristine GF, CNT/GF, and BP-GF electrodes was 94.6, 1,256.4, and 1,547.9 mF g^{-1}, respectively. This indicates that DLC shows a similar trend to BET measurement, confirming that the actual electrochemical surface area of BP-GF electrode is largest. Moreover, as already expected, although the same amount of CNT was loaded onto CNT/GF and BP-GF electrodes, DLC of BP-GF electrode was higher than that of CNT/GF electrode by 23%, implying that CNTs were more efficiently dispersed in BP-GF electrode.

2. Effects of Electrodes on Redox Reactivity of Vanadium Ions and VRFB Performance

The previous evaluations verified that BP-GF electrode was well formed. More specifically, its electrochemical and physical surface area increased and this was due to the uniform dispersion of CNTs loaded onto GF electrode. Moreover, the pore volume of BP-GF electrode was also well configured. It is expected that these characteristics will positively affect the redox reactivity of vanadium ions that are the active material for the operation of actual VRFBs. To confirm whether such BP-GF electrode played a role in improving the redox reactivity of vanadium ions, reactivity of the three electrodes (pristine GF, CNT/GF and BP-GF) was examined electrochemically by measuring their CV curves (Fig. 4).

Such CV curves were measured for both anolyte and catholyte of VRFB. According to Fig. 4, BP-GF electrode showed a higher level of peak current than pristine GF and CNT/GF electrodes.

Quantitatively, in catholyte, the peak current of BP-GF electrode increased more than that of CNT/GF and GF electrodes by 46 and 143%, respectively, while the differences were 10 and 50% in anolyte. Since the condition of electrolyte is same, this result indicates that currents in both electrolytes depend on electrode.

When the results obtained so far are summarized, in both CNT/GF and BP-GF electrodes, active area increased by doping CNTs, and this further induced in the enhancement in redox reactivity of vanadium ions. In a comparison of CNT/GF and BP-GF electrodes, due to the difference in CNT dispersion (Fig. 2 and Table 1), when BP-GF electrode was used, redox reactivity of vanadium ions in-

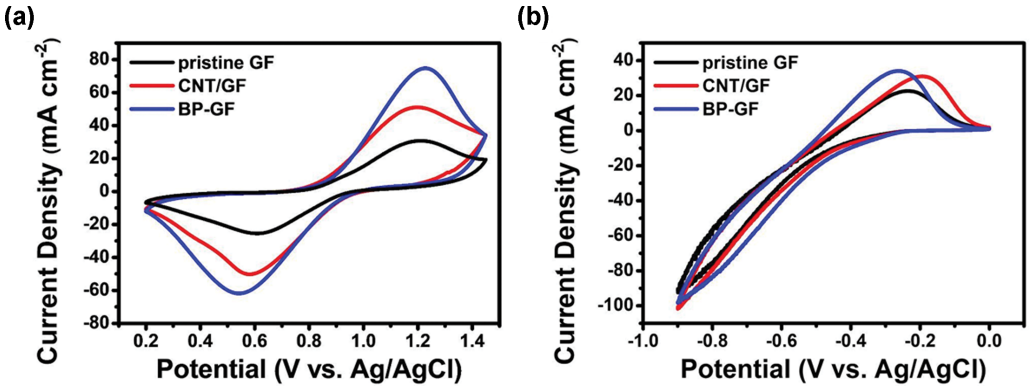

Fig. 4. CV graphs of pristine GF, CNT/GF, and BP-GF electrodes representing (a) VO^{2+}/VO_2^+ redox reaction measured under 0.15 M $VOSO_4$+3 M H_2SO_4 at 50 mV s^{-1} and (b) V^{2+}/V^{3+} redox reaction measured under 0.15 M $VOSO_4$+3 M H_2SO_4 at 50 mV s^{-1}.

Table 3. Performance evaluation of VRFB single cells using three electrodes

Average values		80 mA cm^{-2}	120 mA cm^{-2}	160 mA cm^{-2}	200 mA cm^{-2}
Voltage efficiency (%)	Pristine GF	67.65	53.33	-	-
	CNT/GF	79.72	68.35	55.78	-
	BP-GF	81.75	72.37	64.49	60.39
Coulombic efficiency (%)	Pristine GF	94.97	97.05	-	-
	CNT/GF	94.84	94.78	94.25	-
	BP-GF	94.66	94.42	94.98	95.91
Energy efficiency (%)	Pristine GF	63.79	48.25	-	-
	CNT/GF	74.72	64.27	50.85	-
	BP-GF	76.49	67.83	60.40	51.84
Discharge capacity (Ah L^{-1})	Pristine GF	15.82	3.15	-	-
	CNT/GF	24.80	16.80	4.94	-
	BP-GF	25.83	20.67	14.58	6.20

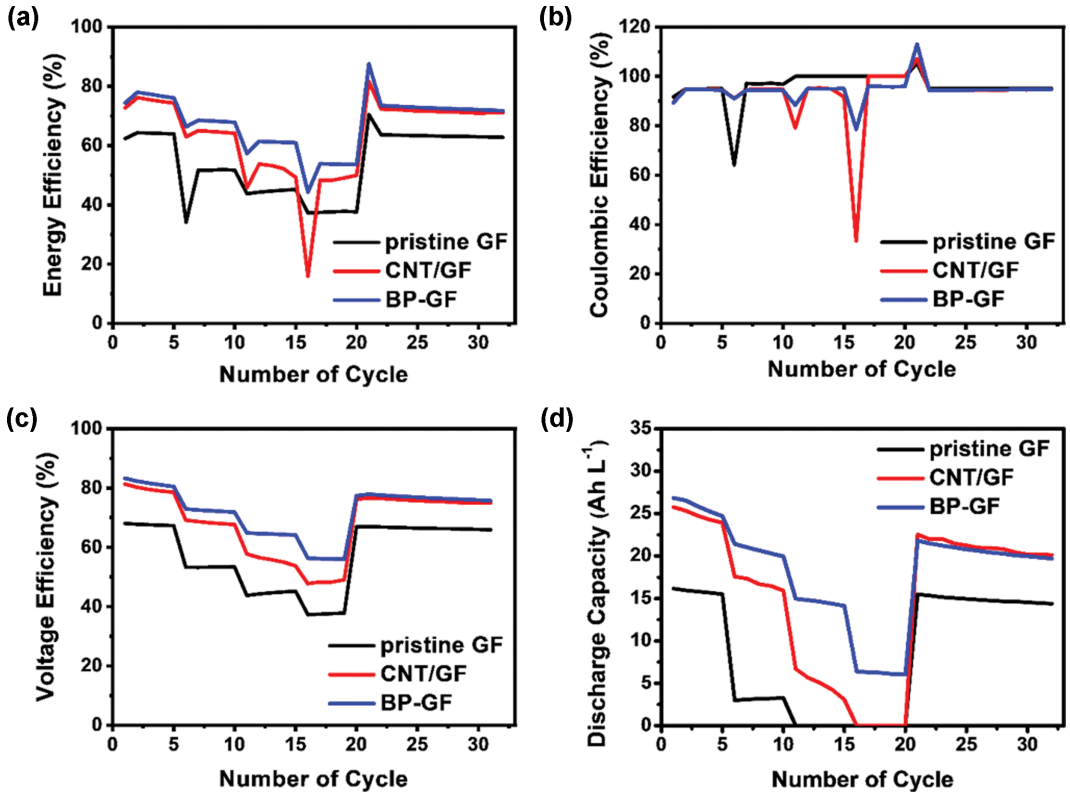

Fig. 5. (a) Energy efficiency, (b) coulombic efficiency, (c) voltage efficiency and (d) discharge capacity graphs of VRFBs using pristine GF, CNT/GF and BP-GF electrodes measured by the step tests of 80 mA cm^{-2} (1-5 cycles), 120 mA cm^{-2} (6-10 cycles), 160 mA cm^{-2} (10-15 cycles), 200 mA cm^{-2} (16-20 cycles) and 80 mA cm^{-2} (21-31 cycles).

creased. Once again, this is because CNTs are efficiently dispersed in BP-GF electrode and, thus, redox reactivity of vanadium ions was promoted.

Next, charge and discharge tests using the related VRFB single cells were conducted to measure the effect of electrochemical active area on the performance of VRFB single cells. In the tests, the performance parameters of VRFB single cells, such as efficiency and capacity, were measured with the change in current density. As test sequence, current density was changed every five cycles, and this was raised to 80, 120, 160, and 200 mA cm^{-2}, and finally returned to its initial value (80 mA cm^{-2}). Then, the tests were conducted for another ten cycles to evaluate the stability of VRFB single cells (Fig. 5, Table 3).

According to Fig. 5, the performance of VRFB single cell using BP-GF electrode was best. VRFB single cell using CNT/GF electrode also showed excellent performance at low current density region. However, when CNT/GF electrode was used, the performance of the VRFB were significantly decreased as current density increased. Even in a high current density region of 200 mA cm^{-2}, VRFB single cell using BP-GF electrode was well operated, whereas that using CNT/GF electrode did not work. For the VRFB single cell using CNT/GF electrode, the maximum operable current density was 160 mA cm^{-2}. More quantitative prospect, when 160 mA cm^{-2} was applied, energy efficiency and capacity of VRFB single cell using CNT/GF electrode were 50.9% and 4.9 Ah L^{-1}, while those of VRFB single cell using BP-GF electrode were 60.4% and 14.6 Ah L^{-1}. Furthermore, when 200 mA cm^{-2} was applied for VRFB single cell test using BP-GF electrode, the operation of the VRFB was possible even if its capacity was only 6.20 Ah L^{-1}. Such different performance of VRFBs using CNT/GF and BP-GF electrodes is due to the increased electrochemical surface area of BP-GF electrode and its CNT utilization.

There was one noticeable thing in Fig. 5. During the data collection, spikes in CE and EE were observed. In our expectation, these spikes might occur during a rapid current density change and the CE and EE were well stabilized in subsequent cycles performed at a constant current density.

CONCLUSIONS

We have suggested the use of thin GF-BP as a new electrode for zero-gap VRFBs. By use of the zero-gap structure for VRFBs, the distance between two electrodes is reduced considerably, while performance and design flexibility of the VRFBs are improved. Here, GF and BP are used as base and reinforced materials to combine the proper porous structure of GF and the excellent redox reactivity of vanadium ions promoted by BP. For clarifying the benefits of thin GF-BP electrode, the properties of the electrode and its applicability to VRFBs were evaluated. According to the evaluations, total pore volume and double layer capacitance of GF-BP electrode (0.200 cm^3 g^{-1}, 1,547.95 mF g^{-1}) were higher than those of pristine GF electrode (0.040 cm^3 g^{-1}, 94.59 mF g^{-1}). Then, in actual VRFB

single cell evaluations, the performance of the zero-gap VRFBs using the optimized GF-BP electrode was excellent with EE of 60% and discharge capacity of 14.6 Ah L^{-1} at 160 mA cm^{-2}. It was revealed that the performance enhancement of the zero-gap VRFBs using GF-BP electrode was due to the large increase in actual active sites of the optimized GF-BP electrode and its CNT utilization.

ACKNOWLEDGEMENT

This study was supported by the Research Program funded by the SeoulTech (Seoul National University of Science and Technology).

REFERENCES

1. K. Hyun, S. Kim and Y. Kwon, *Korean J. Chem. Eng.*, **38**, 2347 (2021).
2. W. Lee, C. Jo, S. Youk, H. Y. Shin, J. Lee, Y. Chung and Y. Kwon, *Appl. Surf. Sci.*, **429**, 187 (2018).
3. M. A. Basit, S. Dilshad, R. Badar and S. M. Sami ur Rehman, *Int. J. Energy Res.*, **44**, 4132 (2020).
4. M. Shin, C. Noh, Y. Chung, D. H. Kim and Y. Kwon, *Appl. Surf. Sci.*, **550**, 148977 (2021).
5. M. Mahmoud, M. Ramadan, A.-G. Olabi, K. Pullen and S. Naher, *Energy Convers. Manag.*, **210**, 112670 (2020).
6. Y. Li, Q. Fu, H. Qin, K. Yang, J. Lv, Q. Zhang, H. Zhang, F. Liu, X. Chen and M. Wang, *Korean J. Chem. Eng.*, **38**, 2113 (2021).
7. M. Shin, S. Oh, H. Jeong, C. Noh, Y. Chung, J. W. Han and Y. Kwon, *Int. J. Energy Res.*, **46**, 8175 (2022).
8. E. Lim, J. Chun, C. Jo and J. Hwang, *Korean J. Chem. Eng.*, **38**, 227 (2021).
9. H. H. Oh and J. Joo, *Korean J. Chem. Eng.*, **38**, 1052 (2021).
10. S. H. Kim, Y. R. Choi, Y. J. Cho, S. Y. Rhyu and S. W. Kang, *Korean J. Chem. Eng.*, **38**, 1715 (2021).
11. N. Jang, W. Kim, D. Lee, G. Yoon, J. Yang, I. Cho, H. Jeon and J. Koo, *Korean J. Chem. Eng.*, **38**, 2397 (2021).
12. J. Lee, Y. Lee, S. Kim, E. E. Kwon and K.-Y. A. Lin, *Korean J. Chem. Eng.*, **38**, 1079 (2021).
13. S. Oh, C. Noh, M. Shin and Y. Kwon, *Int. J. Energy Res.*, **46**, 8803 (2022).
14. C. Noh, S. Moon, Y. Chung and Y. Kwon, *J. Mater. Chem. A*, **5**, 21334 (2017).
15. C. Noh, C. S. Lee, W. S. Chi, Y. Chung, J. H. Kim and Y. Kwon, *J. Electrochem. Soc.*, **165**, A1388 (2018).
16. D. H. Hyeon, J. H. Chun, C. H. Lee, H. C. Jung and S. H. Kim, *Korean J. Chem. Eng.*, **32**, 1554 (2015).
17. C. Noh, D. Serhiichuk, N. Malikah, Y. Kwon and D. Henkensmeier, *Chem. Eng. J.*, **407**, 126574 (2021).
18. M. Jung, W. Lee, N. Nambi Krishnan, S. Kim, G. Gupta, L. Komsiyska, C. Harms, Y. Kwon and D. Henkensmeier, *Appl. Surf. Sci.*, **450**, 301 (2018).
19. W. Lee, A. Permatasari, B. W. Kwon and Y. Kwon, *Chem. Eng. J.*, **358**, 1438 (2019).
20. C. Chu, B. W. Kwon, W. Lee and Y. Kwon, *Korean J. Chem. Eng.*, **36**, 1732 (2019).
21. Y. Shi, C. Eze, B. Xiong, W. He, H. Zhang, T. M. Lim, A. Ukil and J. Zhao, *Appl. Energy*, **238**, 202 (2019).
22. J. Noack, N. Roznyatovskaya, T. Herr and P. Fischer, *Angew. Chemie Int. Ed.*, **54**, 9776 (2015).
23. S. Zhong and M. Skyllas-Kazacos, *J. Power Sources*, **39**, 1 (1992).
24. D. S. Aaron, Q. Liu, Z. Tang, G. M. Grim, A. B. Papandrew, A. Turhan, T. A. Zawodzinski and M. M. Mench, *J. Power Sources*, **206**, 450 (2012).
25. H. O'Connor, J. J. Bailey, O. M. Istrate, P. A. A. Klusener, R. Watson, S. Glover, F. Iacoviello, D. J. L. Brett, P. R. Shearing and P. Nockemann, *Sustain. Energy Fuels*, **6**, 1529 (2022).
26. A. Parra-Puerto, J. Rubio-Garcia, M. Markiewicz, Z. Zheng and A. Kucernak, *ChemElectroChem*, **9**, e202101617 (2022).
27. C. Noh, M. Shin and Y. Kwon, *J. Power Sources*, **520**, 230810 (2022).
28. M. Shin, C. Noh, Y. Chung and Y. Kwon, *Chem. Eng. J.*, **398**, 125631 (2020).
29. C. Noh, B. W. Kwon, Y. Chung and Y. Kwon, *J. Power Sources*, **406**, 26 (2018).
30. R. Phillips and C. W. Dunnill, *RSC Adv.*, **6**, 100643 (2016).
31. S. Abbas, S. Mehboob, H. J. Shin, O. H. Han and H. Y. Ha, *Chem. Eng. J.*, **378**, 122190 (2019).
32. J. Hnát, R. Kodým, K. Denk, M. Paidar, J. Žitka and K. Bouzek, *Chemie Ing. Tech.*, **91**, 821 (2019).
33. W. H. Lee, C. Lim, S. Y. Lee, K. H. Chae, C. H. Choi, U. Lee, B. K. Min, Y. J. Hwang and H.-S. Oh, *Nano Energy*, **84**, 105859 (2021).
34. L. Zeng, Y. Ren, L. Wei, X. Fan and T. Zhao, *Energy Technol.*, **8**, 2000592 (2020).
35. Z. Xu, W. Xiao, K. Zhang, D. Zhang, H. Wei, X. Zhang, Z. Zhang, N. Pu, J. Liu and C. Yan, *J. Power Sources*, **450**, 227686 (2020).
36. L. Wei, C. Xiong, H. R. Jiang, X. Z. Fan and T. S. Zhao, *Energy Storage Mater.*, **25**, 885 (2020).
37. C. Bunte, L. Hussein and G. A. Urban, *J. Power Sources*, **247**, 579 (2014).
38. R. C. Reid, S. D. Minteer and B. K. Gale, *Biosens. Bioelectron.*, **68**, 142 (2015).
39. K. MacVittie, T. Conlon and E. Katz, *Bioelectrochemistry*, **106**, 28 (2015).
40. I. Mustafa, I. Lopez, H. Younes, R. A. Susantyoko, R. A. Al-Rub and S. Almheiri, *Electrochim. Acta*, **230**, 222 (2017).
41. S. Zhang, Y. Ma, L. Suresh, A. Hao, M. Bick, S. C. Tan and J. Chen, *ACS Nano*, **14**, 9282 (2020).
42. K. Chu, C. Jia, W. Li and P. Wang, *Phys. Status Solidi*, **210**, 594 (2013).
43. Y. Wei, L.-M. Luo, H.-B. Liu, X. Zan, J.-P. Song, Q. Xu, X.-Y. Zhu and Y.-C. Wu, *Mater. Des.*, **191**, 108635 (2020).
44. S. R. Sivakkumar, J. M. Ko, D. Y. Kim, B. C. Kim and G. G. Wallace, *Electrochim. Acta*, **52**, 7377 (2007).
45. T. Han, Y. Xiao, M. Tong, H. Huang, D. Liu, L. Wang and C. Zhong, *Chem. Eng. J.*, **275**, 134 (2015).
46. M. Shin, C. Noh and Y. Kwon, *Int. J. Energy Res.*, **46**, 6866 (2022).
47. M. Jung, W. Lee, C. Noh, A. Konovalova, G. S. Yi, S. Kim, Y. Kwon and D. Henkensmeier, *J. Membr. Sci.*, **580**, 110 (2019).
48. Y. Chung, C. Noh and Y. Kwon, *J. Power Sources*, **438**, 227063 (2019).
49. W. Lee, G. Park, D. Schröder and Y. Kwon, *Korean J. Chem. Eng.*, **38**, 1 (2022).
50. P. Mazur, J. Mrlik, J. Pocedic, J. Vrana, J. Dundalek, J. Kosek and T. Bystron, *J. Power Sources*, **414**, 354 (2019).